Metabolic resting-state brain networks in health and disease

Phoebe G. Spetsieris, Ji Hyun Ko, Chris C. Tang, Amir Nazem, Wataru Sako, Shichun Peng, Yilong Ma, Vijay Dhawan, and David Eidelberg[1]

Center for Neurosciences, The Feinstein Institute for Medical Research, Manhasset, NY 11030

Edited* by Joanna S. Fowler, Brookhaven National Laboratory, Upton, NY, and approved January 7, 2015 (received for review June 17, 2014)

The delineation of resting state networks (RSNs) in the human brain relies on the analysis of temporal fluctuations in functional MRI signal, representing a small fraction of total neuronal activity. Here, we used metabolic PET, which maps nonfluctuating signals related to total activity, to identify and validate reproducible RSN topographies in healthy and disease populations. In healthy subjects, the dominant (first component) metabolic RSN was topographically similar to the default mode network (DMN). In contrast, in Parkinson's disease (PD), this RSN was subordinated to an independent disease-related pattern. Network functionality was assessed by quantifying metabolic RSN expression in cerebral blood flow PET scans acquired at rest and during task performance. Consistent task-related deactivation of the "DMN-like" dominant metabolic RSN was observed in healthy subjects and early PD patients; in contrast, the subordinate RSNs were activated during task performance. Network deactivation was reduced in advanced PD; this abnormality was partially corrected by dopaminergic therapy. Time-course comparisons of DMN loss in longitudinal resting metabolic scans from PD and Alzheimer's disease subjects illustrated that significant reductions appeared later for PD, in parallel with the development of cognitive dysfunction. In contrast, in Alzheimer's disease significant reductions in network expression were already present at diagnosis, progressing over time. Metabolic imaging can directly provide useful information regarding the resting organization of the brain in health and disease.

default mode network | resting state networks | PET | principal component analysis | neurodegeneration

The persistence of local brain function in the absence of focused cognitive activity has attracted much interest over the past decade (1–3). Functional MRI (fMRI) is the most commonly used method to identify resting-state functional brain networks (RSNs), particularly the default mode network (DMN). Because of the spatiotemporal complexity of resting-state fMRI recordings, the extraction of stable RSN topographies using this technique has had to rely on processing algorithms, such as independent component analysis (ICA), to isolate discrete sources of signal in the data. Although this approach has delineated consistent patterns of resting activity in healthy populations (4–6), few validated methods exist to quantify and compare the expression of specific RSNs in individual subjects. Such measurements are particularly relevant in the study of progressive neurodegenerative disorders, in which stereotyped abnormalities develop selectively over time in one or another neural system (7). Indeed, associations between new network topographies and previously reported RSNs, particularly the DMN, have often been descriptive (8–10). In this vein, seed-based functional connectivity measurements have been used to delineate areas correlating with activity profiles in a specific nodal region. Regions identified by this method, however, may not exhibit the significant functional intercorrelations that define connected brain networks (11). Moreover, although it is known that regional RSN components can be activated during task performance (12), quantitative techniques are not available for the direct assessment of RSN activity in individual subjects scanned in the resting state and under different task conditions.

In this study, we explored an alternative means of identifying reliable network topographies in the resting state, without the temporal variation in brain signals inherent to fMRI techniques. In the mammalian brain, a substantial portion of resting glucose consumption is dedicated to the support of synaptic activity (13, 14). Thus, FDG PET may be used to map resting brain function in a complementary manner to fMRI. Spatial covariance analysis (15–17) was applied to resting-state metabolic scans from healthy subjects to identify reliable normal RSN topographies, which were then used to quantify pattern expression in individual subjects on a prospective single scan basis. These computations were used to validate the newly identified RSNs in independent testing samples scanned at rest or during task performance. Following validation, we used independent cohorts of Parkinson's disease (PD) and Alzheimer's disease (AD) patients to determine whether normal metabolic RSN topographies are maintained in the setting of ongoing neurodegenerative pathology.

Significance

We present an innovative approach to evaluate default mode network (DMN) activity in individual subjects using metabolic imaging. After characterizing a distinct set of metabolic resting state networks (RSNs) in healthy subjects, network activity was tracked over time in patients with neurodegenerative disorders, such as Parkinson's disease and Alzheimer's disease. We found that the dominant normal metabolic RSN, which corresponded to the DMN, is preserved in early-stage Parkinson's disease patients. Although significant DMN reductions developed later, these changes were reversible in part by dopamine treatment. This finding contrasts with Alzheimer's disease, in which DMN loss is rapid and continuous, beginning before clinical diagnosis. Metabolic imaging can provide a versatile, quantitative means of assessing brain disease at the network level.

Author contributions: P.G.S. and D.E. designed research; P.G.S., J.H.K., C.C.T., A.N., W.S., S.P., Y.M., and V.D. performed research; P.G.S., J.H.K., C.C.T., A.N., and W.S. analyzed data; P.G.S., J.H.K., C.C.T., and D.E. wrote the paper; V.D. supervised the imaging studies; and D.E. supervised the conduct of the research.

Conflict of interest statement: D.E. serves on the scientific advisory boards for and has received honoraria from the Michael J. Fox Foundation for Parkinson's Research and the Bachmann-Strauss Dystonia and Parkinson Foundation; serves on the editorial board of *Annals of Neurology* and *NeuroImage* and as Associate Editor for the *Journal of Neuroscience*; and is listed as coinventor of patents re: Markers for use in screening patients for nervous system dysfunction and a method and apparatus for using same, without financial gain; has received research support from the NIH (National Institute of Neurological Disorders and Stroke, National Institute on Deafness and Other Communication Disorders, National Institute of Allergy and Infectious Diseases), the Dana Foundation, the Bachmann-Strauss Dystonia and Parkinson Foundation, and CHDI Foundation, Inc.; and has served as a consultant for Pfizer.

*This Direct Submission article had a prearranged editor.

[1]To whom correspondence should be addressed. Email: david1@nshs.edu.

This article contains supporting information online at www.pnas.org/lookup/suppl/doi:10.1073/pnas.1411011112/-/DCSupplemental.

Results

Metabolic RSNs: Identification and Spatial Correlation. Spatial covariance analysis of the resting-state metabolic scan data revealed several RSN topographies that were common to the healthy (NL1 and NL2) and disease (PD1) groups (Table S1, *Derivation sets*). The first three principal component patterns (PC1, PC2, PC3) for the NL1 and NL2 groups [NL1: $n = 30$, male/female (M/F) 13/17, age 51.5 ± 14.3 y (mean ± SD); NL2: $n = 33$, M/F 17/16, age 49.8 ± 20.7 y] are displayed in Fig. 1 *A* and *B*. Voxel-wise correlation analysis of the corresponding patterns from the two groups was conducted within an inclusive gray matter mask and presented in descending order according to eigenvalue. The dominant covariance PC1 topography accounted for 14.1% and 16.4% of the subject × voxel variance in the respective derivation samples. The results showed significant cross-correlations (Fig. 1) between the voxel weights on the corresponding topographies identified in the two healthy samples (PC1: $r^2 = 0.61$, $P < 0.001$; PC2: $r^2 = 0.52$, $P < 0.001$; PC3: $r^2 = 0.40$, $P < 0.001$; Pearson's correlations over all voxels $|z| > 0$). Correlations between noncorresponding topographies (e.g., NL1-PC1 and NL2-PC2) were weak at best ($0.003 < r^2 < 0.14$). In addition, the expression scores of the PC1 patterns evaluated in the derivation group and prospectively using the pattern derived in the alternate NL group were highly correlated (NL1: $r^2 = 0.89$, $P < 0.001$; NL2: $r^2 = 0.9233$, $P < 0.001$).

The first RSN identified in the two healthy groups (Fig. 1 *A* and *B*, *Left*) was topographically similar to the DMN (Fig. S1*A*, Fig. S2, Table S2), with relative metabolic increases in the posterior cingulate, medial prefrontal cortex, and to some degree, in the precuneus and lateral parietal association regions. In contrast, the second and third metabolic RSNs in these groups (Fig. 1 *A* and *B*, *Center* and *Right*) were characterized mainly by relative increases in primary and auxiliary motor and sensorimotor cortical areas (Fig. S1 *A* and *B*). Of note, NL1-PC2 (Fig. 1*A*, *Center*) involved the supplementary motor area (SMA), postcentral gyrus, and medial parieto-occipital cortex, whereas the NL1-PC3 (Fig. 1*A*, *Right*) involved the SMA, anterior cingulate cortex, and the cerebellar vermis. Similar metabolic topographies were observed for the corresponding NL2-PC2 and PC3 patterns (Fig. 1*B*, *Center* and *Right*). Data on specific relationships between these metabolic RSNs and known functional topographies are presented as *SI Results*. In aggregate, the correlational analysis indicates that the major metabolic RSN topographies are replicable across healthy volunteer groups. Moreover, the cross-correlation results suggest that RSN hierarchy [i.e., topographical order based on effect size (eigenvalue)] is similar for independent groups of normal subjects.

We next determined whether the major metabolic RSNs identified in healthy subjects—and their hierarchy—are altered in the presence of a neurodegenerative process. To this end, we analyzed scan data from PD1, a group of patients with mild-to-moderate PD (PD1: $n = 33$, M/F 22/11, age 57.2 ± 8.2 y, disease duration 9.2 ± 3.6 y). The first three metabolic RSNs identified in this group are displayed in Fig. 1*C*. The second RSN in this group (PD1-PC2), accounting for 12.4% of the subject × voxel variance, topographically resembled the dominant RSN identified in the two normal groups. Significant correlations (Fig. 1) were observed between voxel weights on this pattern and those on NL1-PC1 and NL2-PC1 ($r^2 > 0.46$ and $r^2 > 0.52$ for the two correlations, respectively). Correlations between voxel weights on PD1-PC2 and those on PC2 and PC3 from either normal group were not noteworthy ($r^2 < 0.19$). Thus, the second metabolic RSN identified in PD1 resembled NL1-PC1 (and the similar NL2-PC1), the dominant resting-state topography seen in healthy subjects. In contrast, the dominant metabolic RSN identified in this disease group (PD1-PC1) was represented by an abnormal topography that was not similar to the patterns derived in either of the healthy volunteer samples. Voxel weights on this pattern were at most marginally related ($r^2 < 0.18$) to those on the first five PCs identified in the analysis of either NL1 or NL2 subjects. This RSN (Fig. 1*C*, *Left*), which accounted for 23.1% of the subject × voxel variance, topographically resembled ($r^2 > 0.8$, $P < 0.001$) the PD-related metabolic covariance pattern (PDRP), a metabolic network that is consistently expressed in patients with this disorder (15, 18, 19). Similarly, PD1-PC1 expression was elevated in PD patients and low in healthy subjects, making it an accurate discriminator of PD subjects (e.g., $P = 1.2e^{-7}$ for PD1 vs. NL2 subject scores, Student's *t* test).

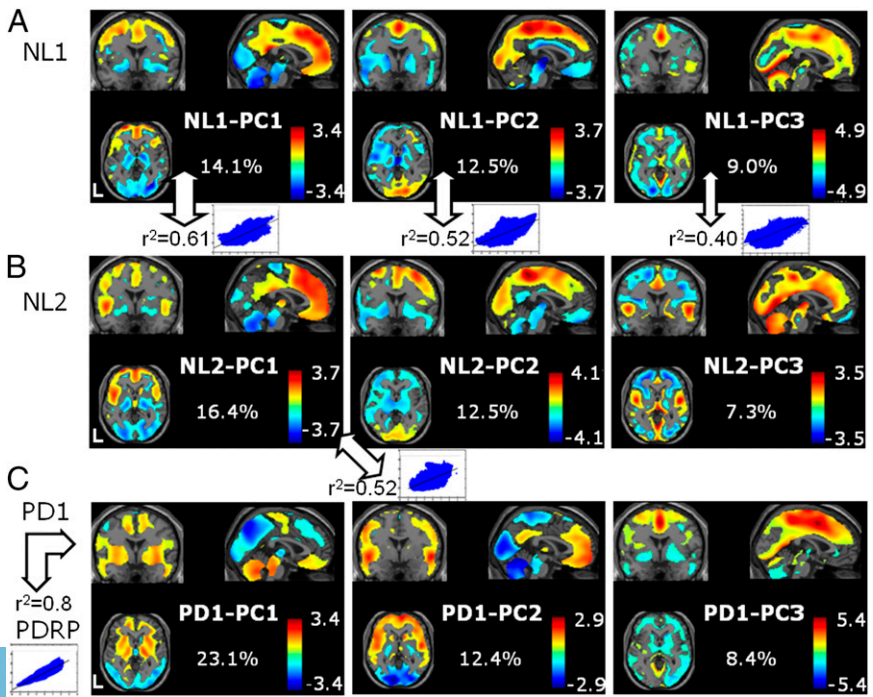

Fig. 1. Metabolic RSNs identified in (*A* and *B*) two groups of healthy volunteer subjects (NL1 and NL2) and (*C*) a group of patients with mild-to-moderate Parkinson's disease (PD1). Region weights (loadings) on each spatial covariance pattern topography are displayed in orthogonal views through the origin of Montreal Neurological Institute (MNI) space (sagittal $X = 0$ mm, coronal $Y = 0$ mm, axial $Z = 0$ mm). The color stripe represents voxel weights on each topography thresholded at $|z| > 0.5$. Arrows indicate significant pairwise correlations ($r^2 \geq 0.40$, $P \leq 0.001$) between nonzero voxel weights ($|z| > 0$) on the two patterns within a common gray matter mask.

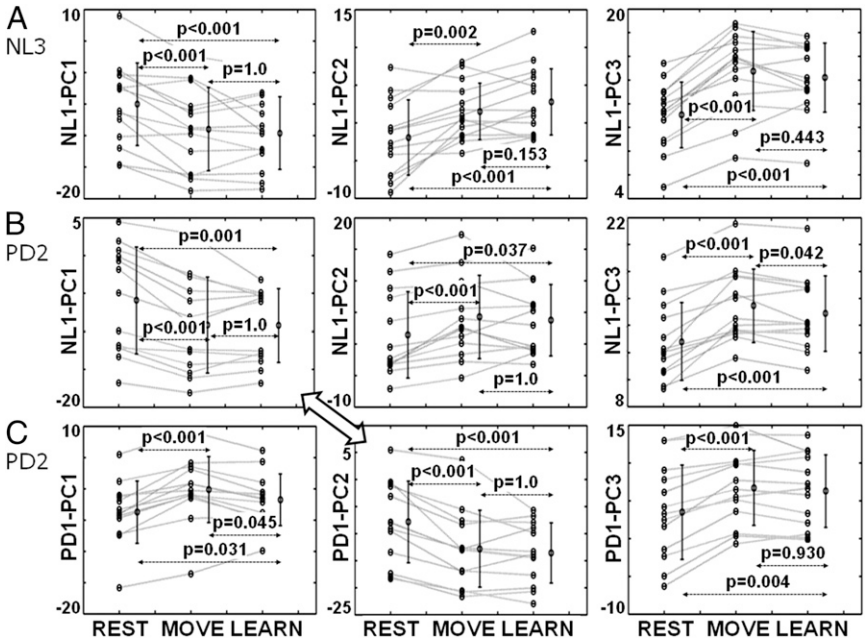

Fig. 2. Metabolic RSN expression values measured at rest (REST) and during motor execution (MOVE) and motor sequence learning (LEARN) in $H_2{}^{15}O$ PET scans from (*A*) healthy subjects (NL3) and (*B*) early-stage PD patients (PD2). In both groups, NL1-PC1 expression (*Left*) was consistently reduced (deactivated) during task performance relative to the nonmovement resting state. Analogous deactivation responses were seen in the early PD group for PD1-PC2 (*C*, *Center*), the second metabolic RSN identified in the PD1 derivation group. The other metabolic RSNs identified in healthy subjects (*A* and *B*, *Center* and *Right*) or in PD patients (*C*, *Left* and *Right*) exhibited consistent increases in expression (activation) during task performance. Significance levels (horizontal arrows) were determined by RMANOVA with post hoc Bonferroni tests.

RSN Activity During Task Performance. Expression values for each metabolic RSN were computed in $H_2{}^{15}O$ PET scans acquired in a nonmovement resting state (REST) and during the performance of the kinematically equivalent motor execution (MOVE) and motor sequence learning (LEARN) tasks. We first confirmed that RSN expression values computed in the resting $H_2{}^{15}O$ PET scans correlated closely with corresponding measurements from FDG PET scans obtained in the same subjects ($r^2 = 0.74$, $P < 0.001$) (Fig. S3). Expression of each metabolic RSN was then computed in the $H_2{}^{15}O$ PET scans obtained in the REST, MOVE, and LEARN conditions in 14 healthy volunteer subjects (NL3: M/F 8/6, age 45.5 ± 16.5 y) and 13 unmedicated early stage PD subjects (PD2: M/F 10/3, age 58.0 ± 10.0 y, disease duration 2.6 ± 1.9 y) (Table S1, *Activation studies*). Consistent relationships (Fig. 2 *A* and *B*) between changes in experimental condition and RSN expression were present in the two groups [NL3: $F_{(4,\ 52)} = 32.3$; PD2: $F_{(4,\ 48)} = 18.1$, $P < 0.001$; task × network interaction effect, repeated-measures ANOVA (RMANOVA)]. Specifically, significant changes in NL1-PC1 expression (Fig. 2 *A* and *B*, *Left*) were observed across the three conditions in both groups [NL3: $F_{(2,\ 26)} = 21.292$, $P < 0.001$; PD2: $F_{(2,\ 24)} = 17.890$, $P < 0.001$; one-way RMANOVA], with reductions in network activity during the performance of either task ($P < 0.001$ for MOVE and LEARN relative to REST; post hoc Bonferroni tests). Measurements of NL1-PC1 expression during the MOVE and LEARN tasks did not differ in either of the two groups ($P = 1.0$). NL1-PC1 deactivation responses in early-stage PD (Fig. 2*B*, *Left*) did not differ from normal [group × task interaction effect: $F_{(2,\ 50)} = 0.803$, $P = 0.454$; 2 × 3 RMANOVA]. In contrast, NL1-PC2 and NL1-PC3 expression increased during task performance in the two groups ($P < 0.001$; one-way RMANOVA). As expected, based on the topographic similarity of PD1-PC2 to NL1-PC1 (Fig. 1), significant deactivation of the former network was observed during both MOVE and LEARN task performance ($P < 0.001$ relative to REST; post hoc Bonferroni tests) (Fig. 2*C*, *Center*). Moreover, at the subject level deactivation responses for PD1-PC2 correlated closely with those for NL1-PC1 [MOVE–REST: $r^2 = 0.73$, $P < 0.0001$, LEARN–REST: $r^2 = 0.79$, $P < 0.0001$ ($n = 13$); Pearson's correlations].

Task-Related RSN Modulation in PD: Natural History and Treatment Effects. Expression values for the three major normal metabolic RSNs (NL1-PC1, -PC2, and -PC3) were computed in $H_2{}^{15}O$ PET scans from a group of 14 later-stage PD patients (PD3: M/F 11/3; age 57.6 ± 7.6 y; disease duration 11.7 ± 4.9 y). These subjects (Table S1, *Activation studies*) were scanned at rest and during task performance in the baseline unmedicated (off) state and in the treated (on) state during intravenous levodopa administration. In the unmedicated state, NL1-PC1 values for these subjects (Fig. 3*A*) did not change significantly across conditions [$F_{(2,\ 26)} = 2.282$, $P = 0.122$; one-way RMANOVA]. This differed [$F_{(2,\ 50)} = 7.555$, $P = 0.001$; group × task interaction effect, two-way RMANOVA] from the robust task-related deactivation seen in early PD (Fig. 2*B*, *Left*), in which significant NL1-PC1 deactivation was present during both movement and learning ($P < 0.002$, MOVE and LEARN relative to REST; post hoc Bonferroni tests). Thus, significant network deactivation during movement was not present in later-stage PD3 patients scanned in the unmedicated state ($P = 1.0$ for MOVE relative to REST; post hoc Bonferroni tests). Indeed, in these subjects, mean

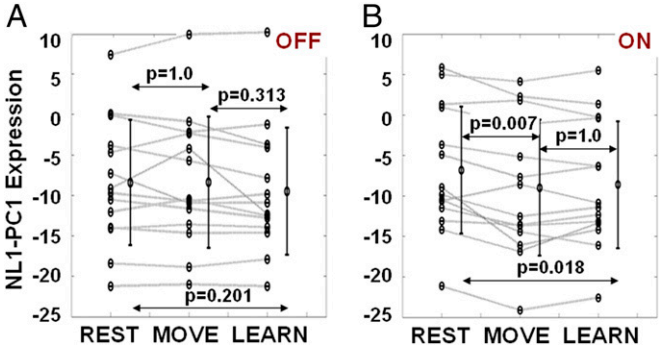

Fig. 3. (*A*) Task-related NL1-PC1 deactivation responses were not observed in unmedicated patients with advanced PD who were scanned with $H_2{}^{15}O$ PET at rest (REST) and during motor execution (MOVE) and sequence learning (LEARN) task performances. This finding contrasted with corresponding measurements in early stage-PD subjects (Fig. 2*B*, *Left*) in whom significant deactivation was observed during both movement and learning. (*B*) Network deactivation was partially restored when the same patients were rescanned on levodopa treatment. Significance levels (horizontal arrows) were determined by RMANOVA with post hoc Bonferroni tests.

NL1-PC1 expression values were similar for the movement and rest conditions (Fig. S4, intersecting lines) when measured in the absence of drug. Although NL1-PC1 motor deactivation was significantly reduced in the unmedicated PD3 group relative to early stage PD and healthy control subjects [PD3 vs. PD2: $F_{(1, 25)} = 17.717$, $P < 0.001$; PD3 vs. NL3: $F_{(1, 26)} = 15.509$, $P < 0.001$, group × task interaction effects; 2 × 2 RMANOVA], this response was partially restored (Fig. 3*B*) by dopaminergic treatment. Specifically, levodopa acted to increase resting RSN expression toward normal (Fig. S4), while reducing the level of network activity recorded during movement. Thus, task-related network modulation was improved by levodopa [$F_{(1, 13)} = 9.461$, $P = 0.009$; treatment × task interaction, RMANOVA], with greater network deactivation responses with treatment [$(\text{MOVE–REST})_{\text{ON}} = -2.175 \pm 0.579$ (mean ± SE), $P = 0.007$] relative to the unmedicated state [$(\text{MOVE–REST})_{\text{OFF}} = 0.025 \pm 0.593$, $P = 1.0$]. In aggregate, this resulted in an increase in the magnitude of the motor deactivation response (Fig. S4, vertical dashed arrows) toward normal levels [$(\text{MOVE–REST})_{\text{NL}} = -3.955 \pm 0.8186$, $P < 0.001$]. Levodopa treatment had an analogous effect on NL1-PC1 deactivation during learning performance.

Metabolic RSNs in the Study of Neurodegenerative Disorders.

Parkinson's disease. Resting NL1-PC1 expression was measured in a group of early-stage PD subjects ($n = 15$, M/F 11/4, age 58.0 ± 10.2 y, disease duration <2 y) who were scanned longitudinally with FDG PET at baseline, 2 y, and 4 y (Table S1, *PD testing sets*). The resulting values were compared with corresponding measurements from a group of healthy volunteer subjects ($n = 15$, M/F 8/7, age 55.8 ± 8.8 y) scanned at a single time point. Network expression in the PD progression cohort (Fig. 4*B*, gray bars) did not differ significantly from control values at any of the longitudinal time points ($P > 0.13$; Student's *t* tests). A declining trend in NL1-PC1 expression was noted over time in the patient group, albeit not reaching significance [$F_{(2, 23)} = 2.60$, $P = 0.10$; one-way RMANOVA]. In a group of more advanced PD patients ($n = 15$, M/F 8/7, age 56.7 ± 12.4 y, disease duration >5 y) with mild cognitive impairment network values (Fig. 4*B*, black bar) were reduced relative to healthy subjects ($P < 0.01$, Student's *t* test).

The time course of NL1-PC1 expression in early PD patients differed significantly from that for the abnormal PDRP network [network × time interaction effect: $F_{(2, 23)} = 5.88$, $P < 0.01$; two-way RMANOVA]. PDRP expression in the early PD cohort (Fig. 4*A*, gray bars) was significantly elevated at baseline ($P < 0.05$) and at each of the subsequent time points ($P < 0.001$, compared with the age-matched healthy subjects; Student's *t* tests), with progressively increasing values over time [$F_{(2, 23)} = 12.73$, $P < 0.0005$; one-way RMANOVA]. PDRP expression in the cognitively impaired PD group (Fig. 4*A*, black bar) was further elevated relative to healthy controls ($P < 0.001$, Student's *t* test).

Alzheimer's disease. Progressive changes in resting NL1-PC1 expression were also assessed in early-stage AD patients ($n = 40$, M/F 23/17, age 75.7 ± 6.3 y, disease duration 4.4 ± 2.6 y) and healthy volunteer subjects ($n = 40$, M/F 23/17, age 75.9 ± 4.6 y) scanned longitudinally with FDG PET as part of the Alzheimer's Disease Neuroimaging Initiative (Table S1, *AD testing set*). In both groups, network expression was measured at baseline, 6 mo, 12 mo, and 24 mo. Network expression in the healthy cohort (Fig. 4*D*) did not change significantly over time [$F_{(3, 117)} = 1.21$, $P = 0.31$, one-way RMANOVA)]. In contrast, in the AD group NL1-PC1 expression (Fig. 4*C*) was significantly reduced at each time point (baseline, 6 mo, and 12 mo: $P < 0.05$, 24 mo: $P < 0.01$, Student's *t* tests with respect to normal baseline values). In contrast to the healthy subjects, the AD patients exhibited a progressive decline in network expression over time [$F_{(3, 117)} = 9.67$, $P < 0.0001$; one-way RMANOVA]. Thus, in contrast to PD, AD patients exhibit progressive loss of the DMN-like metabolic network beginning early in the natural history of the disorder.

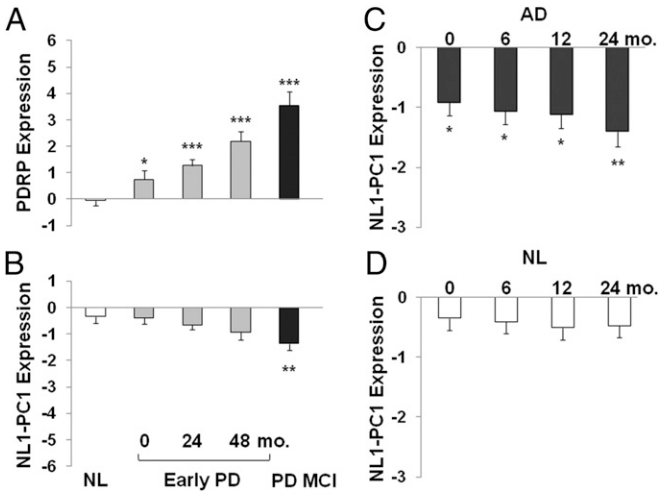

Fig. 4. *Z*-scored expression values are displayed for (*A*) the abnormal PDRP measured in 15 early-stage PD patients (gray bars) scanned longitudinally with FDG PET at baseline, 24 mo, and 48 mo, and (*B*) the dominant metabolic RSN identified in healthy subjects (NL1-PC1). In *A* and *B*, expression values for the two networks are also displayed for 15 later-stage PD patients of similar age with mild cognitive impairment (black bars) and 15 age-matched healthy volunteer subjects (white bars). The two networks exhibited different time courses in members of the early-stage longitudinal PD cohort ($P < 0.01$, network × time interaction effect; RMANOVA). Significant increases in PDRP expression were present over time in these subjects (main effect of time: $P < 0.0005$; one-way RMANOVA), without concurrent change in NL1-PC1 expression ($P = 0.12$). NL1-PC1 expression was reduced, however, in the later-stage PD subjects with cognitive impairment ($P < 0.01$; Student's *t* test with respect to normal control values). (*C*) NL1-PC1 *z*-scored expression values in 40 early-stage AD patients (black bars) scanned with FDG PET at baseline, 6, 12, and 24 mo and (*D*) 40 normal (NL) subjects (white bars). Although NL1-PC1 expression did not change over time in healthy subjects ($P = 0.31$, one-way RMANOVA), a progressive decline in this measure ($P < 0.0001$) was present in the AD group. In the AD group, a significant reduction in the expression of this network was present at each time point ($P < 0.05$, Student's *t* tests with respect to normal baseline values). *$P < 0.05$, **$P < 0.01$, ***$P < 0.001$, Student's *t* tests. Error bar represents SE.

Discussion

In this study, we used a comparatively simple spatial covariance technique to isolate stable, functionally relevant RSN topographies, resembling in some basic features those described previously with resting-state fMRI using fundamentally different methodology. For fMRI networks typically derived from temporal correlation in fluctuations of a small-frequency band of time-dependent data, the variance contribution to the total signal may be negligible. Temporo-spatial fluctuations are absent in the metabolic imaging data because of the time averaging inherent in PET image acquisition. The findings therefore suggest that these networks represent patterns of regional covariation that involve a greater portion of resting-state neuronal activity than previously appreciated. By analyzing total metabolic activity, we identified a set of orthogonal, spatially overlapping networks that describe multifunctional, reproducible components of brain function in the resting state. Thus, the dominant metabolic RSN in healthy subjects, exemplified by NL1-PC1, shared prominent features with previously reported fMRI-based DMN topographies, although the technique of network derivation was notably different for the two imaging modalities. Even so, the PET-derived metabolic network was consistently deactivated during task performance, with few—if any—exceptions at the individual-subject level. The presence of stereotyped task-related deactivation responses for NL1-PC1 suggested that this RSN

may have particular utility as a stable quantitative descriptor of DMN activity in neurodegenerative disorders. It should be noted that deactivation of the metabolic patterns refers to the modulation of the pattern score that is evaluated over the entire brain and not within individual regions, as typically performed in fMRI analysis. The fraction of the total activity measured within a region that is contributed by a particular pattern is proportional to the product of the subject's expression of the pattern and the sum of the pattern's unit-normalized regional voxel weights. Although highly weighted regions may have a greater influence on pattern score, regional values alone are not as predictive as whole covariance pattern expression in performance measures.

In addition to loss of normal DMN activity, the earliest stages of neurodegenerative illnesses are often associated with increasing expression of independent, abnormal disease-related metabolic networks (15, 18, 20, 21). Using our approach, we directly compared the time course of the changes in normal and pathological network activity that occur in patients with these disorders. The utility of this analytical strategy is highlighted by the PD findings. We found that the normal DMN-like topography was expressed in subjects with mild-to-moderate disease [represented by PD1-PC2, 12.4% "variance accounted for" (vaf)]. Nonetheless, this RSN was now subordinated to an aberrant (orthogonal) disease-related pattern (PD1-PC1, 23.1% vaf) not expressed in healthy subjects. Considering that the average vaf attributed to any one PC decreases with the number of subjects, the independent DMN-like component (PD1-PC2) was represented proportionally for sample size ($n = 33$): about half of the contribution of the disease pattern (PD1-PC1) and slightly less than vaf measures for the DMN observed in normal groups of similar size. Indeed, resting NL1-PC1 expression (and NL2-PC1, similarly) did not differ from normal in early-stage PD subjects scanned using either cerebral blood flow or metabolic imaging techniques (Figs. 2 *A* and *B*, and 4*B*, gray bars). In contrast, resting expression of this RSN was significantly reduced in unmedicated later-stage patients scanned using one or the other technique (Figs. 3*A* and 4*B*, black bar). Overall, differences in disease stage and treatment status may explain the inconsistency of prior studies of DMN connectivity and task-related deactivation in PD subjects (22–24). Partial restoration of these responses occurred following levodopa administration (Fig. 3*B* and Fig. S4), perhaps through enhanced dopaminergic neurotransmission in mesolimbic pathway (25, 26).

One would generally not expect the network architecture of the brain to remain intact in the setting of a progressive neurodegenerative process (7). We note that continuing increases in the expression of disease-related metabolic RSNs, such as PDRP (Fig. 4*A*) have been observed in individuals scanned 10–15 y after diagnosis (18, 27, 28). The present findings suggest that these changes occur in parallel with progressive loss of normal RSN functioning (Fig. 4*B*). In this vein, the NL1-PC1 topography accounted for 10.1% in the baseline scans of the early-stage longitudinal PD cohort. Nonetheless, this network accounted for only 6.0% of the variance in the more advanced PD-mild cognitive impairment group. (The corresponding percentage of vaf values for NL2-PC1 were 10.0% and 6.9% for the two groups, respectively.) We also found that levodopa can partially restore DMN function in moderately advanced PD patients (Fig. 3*B* and Fig. S4). In earlier work, we found an association between the effect of levodopa on parkinsonian motor symptoms and concurrent reductions in PDRP expression (18, 29, 30). Indeed, clinically effective levodopa treatment lowered PDRP expression ($P < 0.02$; paired Student's t test) in resting metabolic images from PD3 patients scanned at baseline and with medication. NL1-PC1 "restoration" under these circumstances was modest, however; the normal RSN topography accounted for 6.2% of the subject × voxel variance in the baseline data and 6.9% with treatment. (The corresponding values for NL2-PC1 were 5.4% and 6.1% vaf for the two treatment conditions.) It is likely that with advancing neurodegeneration, connectivity within and between the normal RSNs is further compromised with irreversible loss-of-network functioning. Beyond that point, manipulation of pathological networks is not expected to affect normal RSN functioning in a meaningful way.

The situation in AD is somewhat different in that significant reductions in NL1-PC1 expression were already present at the time of diagnosis (Fig. 4*C*). Indeed, the present findings are fully in line with resting fMRI studies demonstrating DMN abnormalities at the earliest clinical stages of the disorder (31, 32). Nonetheless, the loss of NL1-PC1 expression at diagnosis in AD patients, although greater than analogous changes observed in early PD, was modest in size (between 1.0 and 1.5 SD below the normal mean), particularly given the degree of cognitive impairment that was observed in these individuals. Of note, AD is also associated with a characteristic disease-related metabolic covariance pattern topographically distinct from the DMN, which is expressed in early-stage patients but not in healthy subjects (15, 33). In contrast to the PDRP, the pathological AD network shares several regions with the NL1-PC1 topography, a cause perhaps for the early DMN changes seen in this disorder. Notably little deterioration of DMN expression over time was observed in healthy subjects (Fig. 4*D*). The longitudinal relationship between normal and disease-related RSNs in different neurodegenerative conditions, and their respective roles in the natural history of these disorders, is a topic of ongoing investigation.

The present work illustrates the use of glucose metabolic imaging to assess RSN function under normal and pathological conditions. Distinct replicable topographies were identified that are also physiologically different in regard to task-related network activation responses including NL1-PC1 deactivated by task and NL1-PC2 and NL1-PC3 activated by task. A recent experimental rat study demonstrated the presence of several similar network topographies in healthy animals scanned simultaneously with FDG PET and fMRI (34). Analogous covariance patterns have also been reported following the application of ICA to imaging data from healthy human subjects scanned in the resting state with both modalities (10). However, in contrast to the present findings, a DMN-like topography was not identified when ICA was applied to this FDG PET dataset. Metabolic imaging may be sensitive to the distinct patterns of resting neural activity and energy consumption reported in DMN areas (35). Whether the changes in local cerebral function seen in these regions reflect the activity of a single brain network depends on the criteria for statistical independence used in the underlying models, which differ considerably for ICA and principal component analysis (PCA). Indeed, in the present study, reproducible DMN topographies were identified in resting FDG PET data from several independent populations using a simple PCA-based algorithm. A better understanding of how such metabolic RSNs relate to traditional electrically defined networks may be achieved by correlating multimodal network measurements with local field potentials in experimental animal models.

Methods

A more detailed description of the methods used in this study is provided in *SI Methods*. The Scaled Subprofile Model (SSM-PCA) (36, 37) was used to identify significant resting-state metabolic PC topographies of spatial covariance in two independent NL groups and a PD group (NL1, NL2, PD1) (Table S1, *Derivation sets*) using ScanVP software (www.feinsteinneuroscience.org). The hierarchy of these PC RSNs is established by the decreasing order of the magnitude of their eigenvalue corresponding to the decreasing relative value of the vaf in the data. Thus, the entire dataset analysis is usually reduced to only the first one to five prominent PCs corresponding to normal networks or disease components. The correlation of patterns derived in the independent derivation groups was evaluated as the magnitude (r^2) and corresponding P value of the voxel-wise Pearson product–moment correlation of the two image-weight vectors computed over all nonthresholded voxels ($|z| > 0$). For

voxel-wise correlations between topographies, *P* values were computed incorporating a correction for spatial autocorrelation effects as described previously (38). Furthermore, to validate the correlation of the expression of the two primary normal patterns, we measured the correlation of derivation scores in each normal group with prospective scores for the same group using the alternate normal cohort pattern.

The relationship of the primary metabolic RSN to previous fMRI-based descriptions of the topography of the DMN (39, 40) was examined by localizing within each PC image the primary nodes of the DMN derived in an fMRI consensus study using the published Talairach coordinates: medial prefrontal cortex (mPFC: 1 40 16), left and right lateral parietal areas (LatParL: −45 −67 26, LatParR: 53–65 26), and the posterior cingulate cortex (pCC: −1 −50 26). The reliability of the voxel weights on each RSN was mapped by the inverse coefficient of variation (ICV) determined by bootstrap resampling (500 iterations) of the derivation data for each topography (33, 41). Thresholded ICV values at $|z| > 2.0$ correspond to a significance level of $P < 0.03$.

Using the SSM-PCA model, prospective expression of each pattern was computed individually as a scalar score for each subject in different experimental groups for conditions of activation under movement (Table S1, *Activation studies*) and in degenerative conditions of PD (Table S1, *PD testing sets*) and AD (Table S1, *AD testing set*). RSN expression during task performance in $H_2{}^{15}O$ PET scans was obtained separately for a simple motor execution task (MOVE), a kinematically matched motor sequence learning task (LEARN), and in an eyes-open resting state (REST) for independent sets of healthy subjects (NL3) and unmedicated early stage PD patients (PD2). In addition, more advanced PD subjects (PD3) were scanned with $H_2{}^{15}O$ PET during task performance while off and on intravenous levodopa treatment.

Longitudinal studies of Parkinson's disease were performed for FDG data (Table S1, *PD testing sets*) of early stage subjects scanned at baseline, and again 24 and 48 mo later and compared with healthy and advanced PD subjects. Expression of the major normal pattern NL1-PC1 was compared with the expression of the known PD disease pattern, PDRP. For the AD study, expression of the major normal pattern was compared in healthy and AD subject data obtained from the multicenter Alzheimer's Disease Neuroimaging Initiative database (ida.loni.usc.edu/login.jsp) at baseline, and 6, 12, and 24 mo later (Table S1, *AD testing set*). RSN expression in patients and controls was *z*-scored with respect to corresponding values from the NL1 derivation group.

Statistical analysis was performed using SPSS 13.0 for Windows (SPSS Inc.). Comparisons were considered significant for $P < 0.05$, two-tailed. Differences in RSN expression (subject scores) were compared across groups using Student's *t* test or ANOVA. Comparisons of RSN expression values across groups and experimental conditions, as well as group × condition interaction effects, were assessed using RMANOVA with post hoc Bonferroni tests. RMANOVA was also used to compare longitudinal changes in the expression of normal and disease patterns (e.g., NL1-PC1 vs. PDRP) in the same subjects. To avoid network effects referable solely to subject score sign, we multiplied expression values for the normally decreasing RSN patterns by −1. Thus, expression for normal and disease-related RSNs in individual subjects were modeled as moving longitudinally in the same direction (i.e., progressively increasing with respect to the control mean) but with potentially different trajectories over time.

Study Approval. Ethical permission for these studies was obtained from the Institutional Review Boards at North Shore University Hospital and from the institutions participating in the Alzheimer's Disease Neuroimaging Initiative. Written informed consent was obtained from each subject following detailed explanation of the procedures.

ACKNOWLEDGMENTS. We thank Ms. Ivana De Lucia for her valuable technical assistance, and Ms. Yoon Young Choi and Ms. Toni Fitzpatrick for manuscript preparation/copyediting. This work was supported in part by the National Institute of Neurological Disorders and Stroke Morris K. Udall Center of Excellence for Parkinson's Disease Research at The Feinstein Institute for Medical Research (P50 NS071675) (to D.E.).

1. Raichle ME, Snyder AZ (2007) A default mode of brain function: A brief history of an evolving idea. *Neuroimage* 37(4):1083–1090, discussion 1097–1099.
2. Buckner RL, Andrews-Hanna JR, Schacter DL (2008) The brain's default network: Anatomy, function, and relevance to disease. *Ann N Y Acad Sci* 1124:1–38.
3. Andrews-Hanna JR (2012) The brain's default network and its adaptive role in internal mentation. *Neuroscientist* 18(3):251–270.
4. Damoiseaux JS, et al. (2006) Consistent resting-state networks across healthy subjects. *Proc Natl Acad Sci USA* 103(37):13848–13853.
5. Allen EA, et al. (2011) A baseline for the multivariate comparison of resting-state networks. *Front Syst Neurosci* 5:2.
6. Biswal BB, et al. (2010) Toward discovery science of human brain function. *Proc Natl Acad Sci USA* 107(10):4734–4739.
7. Seeley WW, Crawford RK, Zhou J, Miller BL, Greicius MD (2009) Neurodegenerative diseases target large-scale human brain networks. *Neuron* 62(1):42–52.
8. Sorg C, et al. (2007) Selective changes of resting-state networks in individuals at risk for Alzheimer's disease. *Proc Natl Acad Sci USA* 104(47):18760–18765.
9. Leech R, Kamourieh S, Beckmann CF, Sharp DJ (2011) Fractionating the default mode network: Distinct contributions of the ventral and dorsal posterior cingulate cortex to cognitive control. *J Neurosci* 31(9):3217–3224.
10. Di X, Biswal BB; Alzheimer's Disease Neuroimaging Initiative (2012) Metabolic brain covariant networks as revealed by FDG-PET with reference to resting-state fMRI networks. *Brain Connect* 2(5):275–283.
11. Habeck C, Moeller JR (2011) Intrinsic functional-connectivity networks for diagnosis: Just beautiful pictures? *Brain Connect* 1(2):99–103.
12. Smith SM, et al. (2009) Correspondence of the brain's functional architecture during activation and rest. *Proc Natl Acad Sci USA* 106(31):13040–13045.
13. Hyder F, Fulbright RK, Shulman RG, Rothman DL (2013) Glutamatergic function in the resting awake human brain is supported by uniformly high oxidative energy. *J Cereb Blood Flow Metab* 33(3):339–347.
14. Raichle ME, Mintun MA (2006) Brain work and brain imaging. *Annu Rev Neurosci* 29: 449–476.
15. Eidelberg D (2009) Metabolic brain networks in neurodegenerative disorders: A functional imaging approach. *Trends Neurosci* 32(10):548–557.
16. Habeck C, Stern Y; Alzheimer's Disease Neuroimaging Initiative (2010) Multivariate data analysis for neuroimaging data: Overview and application to Alzheimer's disease. *Cell Biochem Biophys* 58(2):53–67.
17. Spetsieris P, et al. (2013) Identification of disease-related spatial covariance patterns using neuroimaging data. *J Vis Exp* 76(76):e50319.
18. Niethammer M, Eidelberg D (2012) Metabolic brain networks in translational neurology: Concepts and applications. *Ann Neurol* 72(5):635–647.
19. Spetsieris PG, Eidelberg D (2011) Scaled subprofile modeling of resting state imaging data in Parkinson's disease: Methodological issues. *Neuroimage* 54(4):2899–2914.
20. Holtbernd F, et al. (2014) Abnormal metabolic network activity in REM sleep behavior disorder. *Neurology* 82(7):620–627.
21. Tang CC, et al. (2013) Metabolic network as a progression biomarker of premanifest Huntington's disease. *J Clin Invest* 123(9):4076–4088.
22. Delaveau P, et al. (2010) Dopaminergic modulation of the default mode network in Parkinson's disease. *Eur Neuropsychopharmacol* 20(11):784–792.
23. Krajcovicova L, Mikl M, Marecek R, Rektorova I (2012) The default mode network integrity in patients with Parkinson's disease is levodopa equivalent dose-dependent. *J Neural Transm* 119(4):443–454.
24. van Eimeren T, Monchi O, Ballanger B, Strafella AP (2009) Dysfunction of the default mode network in Parkinson disease: A functional magnetic resonance imaging study. *Arch Neurol* 66(7):877–883.
25. Argyelan M, et al. (2008) Dopaminergic suppression of brain deactivation responses during sequence learning. *J Neurosci* 28(42):10687–10695.
26. Mattay VS, et al. (2002) Dopaminergic modulation of cortical function in patients with Parkinson's disease. *Ann Neurol* 51(2):156–164.
27. Feigin A, et al. (2007) Modulation of metabolic brain networks after subthalamic gene therapy for Parkinson's disease. *Proc Natl Acad Sci USA* 104(49):19559–19564.
28. Moeller JR, Eidelberg D (1997) Divergent expression of regional metabolic topographies in Parkinson's disease and normal ageing. *Brain* 120(Pt 12):2197–2206.
29. Asanuma K, et al. (2006) Network modulation in the treatment of Parkinson's disease. *Brain* 129(Pt 10):2667–2678.
30. Mattis PJ, Tang CC, Ma Y, Dhawan V, Eidelberg D (2011) Network correlates of the cognitive response to levodopa in Parkinson disease. *Neurology* 77(9):858–865.
31. Damoiseaux JS, Prater KE, Miller BL, Greicius MD (2012) Functional connectivity tracks clinical deterioration in Alzheimer's disease. *Neurobiol Aging* 33(4):e19–e30.
32. Koch W, et al. (2012) Diagnostic power of default mode network resting state fMRI in the detection of Alzheimer's disease. *Neurobiol Aging* 33(3):466–478.
33. Habeck C, et al. (2008) Multivariate and univariate neuroimaging biomarkers of Alzheimer's disease. *Neuroimage* 40(4):1503–1515.
34. Wehrl HF, et al. (2013) Simultaneous PET-MRI reveals brain function in activated and resting state on metabolic, hemodynamic and multiple temporal scales. *Nat Med* 19(9):1184–1189.
35. Vaishnavi SN, et al. (2010) Regional aerobic glycolysis in the human brain. *Proc Natl Acad Sci USA* 107(41):17757–17762.
36. Alexander GE, Moeller JR (1994) Application of the scaled subprofile model to functional imaging in neuropsychiatric disorders: A principal component approach to modeling brain function in disease. *Hum Brain Mapp* 2(1–2):79–94.
37. Moeller JR, Strother SC (1991) A regional covariance approach to the analysis of functional patterns in positron emission tomographic data. *J Cereb Blood Flow Metab* 11(2):A121–A135.
38. Ko JH, Spetsieris P, Ma Y, Dhawan V, Eidelberg D (2014) Quantifying significance of topographical similarities of disease-related brain metabolic patterns. *PLoS ONE* 9(1): e88119.
39. Bellec P, et al. (2011) Resting-state brain networks in functional MRI. *Brain mapping: from neural basis of cognition to surgical applications*, ed Duffau H (Springer, Wien, Austria), pp 361–372.
40. Habeck C, Steffener J, Rakitin B, Stern Y (2012) Can the default-mode network be described with one spatial-covariance network? *Brain Res* 1468:38–51.
41. Efron B, Tibshirani R (1998) *An Introduction to the Bootstrap* (CRC Press, LLC, New York).